Applied Mathematics Letters 132 (2022) 108161

Contents lists available at ScienceDirect

Applied Mathematics Letters

www.elsevier.com/locate/aml

Energy quadratization Runge–Kutta scheme for the conservative Allen–Cahn equation with a nonlocal Lagrange multiplier

Hyun Geun Lee [a], Jaemin Shin [b], June-Yub Lee [c,*]

[a] Department of Mathematics, Kwangwoon University, Seoul 01897, Republic of Korea
[b] Department of Mathematics, Chungbuk National University, Cheongju 28644, Republic of Korea
[c] Department of Mathematics, Ewha Womans University, Seoul 03760, Republic of Korea

ARTICLE INFO

Article history:
Received 21 February 2022
Received in revised form 26 April 2022
Accepted 26 April 2022
Available online 5 May 2022

Keywords:
Mass conservation
Unconditional energy stability
High-order time accuracy
Invariant energy quadratization
Scalar auxiliary variable

ABSTRACT

In this study, we present a high-order energy stable scheme for the conservative Allen–Cahn equation with a nonlocal Lagrange multiplier by combining the concept of energy quadratization and the Runge–Kutta method. Under the stability condition for the Runge–Kutta coefficients, we analytically demonstrate that the scheme is unconditionally stable with respect to the reformulated energy. Additionally, we develop a Newton-type fixed point iteration method to implement the scheme, enabling the achievement of a fast iterative convergence. Numerical experiments are presented to demonstrate the accuracy and energy stability of the proposed scheme.

© 2022 Elsevier Ltd. All rights reserved.

1. Introduction

Many phase-field equations are given by gradient flows for energy functionals [1,2]. The Allen–Cahn (AC) equation [3] is a L^2-gradient flow for the Ginzburg–Landau energy functional,

$$\mathcal{E}(\phi) = \int_\Omega \left(F(\phi) + \frac{\epsilon^2}{2} |\nabla \phi|^2 \right) d\mathbf{x}, \tag{1}$$

where $\Omega \subset \mathbb{R}^d$ $(d = 1, 2, 3)$, ϕ is the order parameter, $F(\phi) = \frac{1}{4}(\phi^2 - 1)^2$, and $\epsilon > 0$ is a constant related to the interfacial thickness. For the sake of simplicity, we assume the zero Neumann boundary condition for ϕ: $\nabla \phi \cdot \mathbf{n} = 0$ on $\partial\Omega$, where $\mathbf{n}$ is a unit normal vector to $\partial\Omega$. Because the AC equation is of the gradient type, it is easy to see that (1) is nonincreasing in time.

The original AC equation does not conserve the total mass. Hence, we introduce the conservative AC (CAC) equation to overcome this shortcoming by adding a nonlocal Lagrange multiplier to the AC

* Corresponding author.
E-mail address: jyllee@ewha.ac.kr (J.-Y. Lee).

https://doi.org/10.1016/j.aml.2022.108161
0893-9659/© 2022 Elsevier Ltd. All rights reserved.

equation [4], as follows.

$$\frac{\partial \phi}{\partial t} = -\frac{\delta \mathcal{E}}{\delta \phi} + \frac{1}{|\Omega|}\int_\Omega f(\phi)\, d\mathbf{x} = -\left(f(\phi) - \epsilon^2 \Delta \phi\right) + \frac{1}{|\Omega|}\int_\Omega f(\phi)\, d\mathbf{x}, \tag{2}$$

where $\frac{\delta}{\delta \phi}$ denotes the variational derivative and $f(\phi) = F'(\phi)$. The CAC Eq. (2) satisfies the mass conservation and energy dissipation property as expressed below.

$$\frac{d}{dt}\int_\Omega \phi\, d\mathbf{x} = \int_\Omega \frac{\partial \phi}{\partial t}\, d\mathbf{x} = -\int_\Omega \left(f(\phi) - \epsilon^2 \Delta \phi\right) d\mathbf{x} + \int_\Omega f(\phi)\, d\mathbf{x} = 0$$

and

$$\begin{aligned}\frac{d\mathcal{E}}{dt} &= \int_\Omega \frac{\delta \mathcal{E}}{\delta \phi}\frac{\partial \phi}{\partial t}\, d\mathbf{x} = \int_\Omega \left(-\frac{\partial \phi}{\partial t} + \frac{1}{|\Omega|}\int_\Omega f(\phi)\, d\mathbf{x}\right)\frac{\partial \phi}{\partial t}\, d\mathbf{x} \\ &= -\int_\Omega \left(\frac{\partial \phi}{\partial t}\right)^2 d\mathbf{x} + \frac{1}{|\Omega|}\int_\Omega f(\phi)\, d\mathbf{x}\int_\Omega \frac{\partial \phi}{\partial t}\, d\mathbf{x} = -\int_\Omega \left(\frac{\partial \phi}{\partial t}\right)^2 d\mathbf{x} \le 0.\end{aligned}$$

We note that there are many versions of the CAC equation [5–7] that conserve the mass but do not comply with energy properties.

While the mass is conserved precisely, the additional nonlocal Lagrangian term causes difficulties in developing accurate and stable numerical methods for Eq. (2). There are various related works [8–12] but most of them have only first-order time accuracy or are unable to prove energy stability, with the exception of [11,12]. The aim of the present work is to present a high-order energy stable scheme for Eq. (2) by combining the energy quadratization (EQ) concept, such as the invariant energy quadratization (IEQ) [13] and the scalar auxiliary variable (SAV) [14–16], with the Runge–Kutta (RK) method [17]. Under the stability condition for the RK coefficients [18], we analytically demonstrate that the scheme is unconditionally stable with respect to the reformulated energy. Furthermore, we develop a Newton-type fixed point iteration method to implement the scheme, enabling the achievement of a fast iterative convergence.

The rest of this paper is organized as follows. In Section 2, we propose the EQ-RK scheme, prove its unconditional energy stability, and describe its numerical implementation. In Section 3, we present numerical examples demonstrating the accuracy and energy stability of the proposed scheme. Finally, conclusions with the main contribution and results are drawn in Section 4.

2. Energy quadratization Runge–Kutta scheme

2.1. Energy quadratization reformulations

To obtain an EQ reformulation, we utilize the invariant energy quadratization (IEQ) idea by introducing an auxiliary variable $\psi(\mathbf{x}, t) = \sqrt{F(\phi) + C}$, where C is a constant such that $F(\phi) + C > 0$. Then, one can redefine the energy $\mathcal{E}(\phi)$ as

$$\mathcal{E}_{IEQ}(\phi, \psi) = \int_\Omega \left(\psi^2 + \frac{\epsilon^2}{2}|\nabla \phi|^2\right) d\mathbf{x} - C|\Omega| \tag{3}$$

and reformulate Eq. (2) as

$$\frac{\partial \phi}{\partial t} = -\left(G(\phi)\psi - \epsilon^2 \Delta \phi\right) + \frac{1}{|\Omega|}\int_\Omega G(\phi)\psi\, d\mathbf{x}, \quad \frac{\partial \psi}{\partial t} = \frac{1}{2}G(\phi)\frac{\partial \phi}{\partial t}, \tag{4}$$

where $G(\phi) = \frac{f(\phi)}{\sqrt{F(\phi)+C}}$. The new system (4) still satisfies the mass conservation and energy dissipation properties:

$$\frac{d}{dt}\int_\Omega \phi\, d\mathbf{x} = \int_\Omega \frac{\partial \phi}{\partial t}\, d\mathbf{x} = -\int_\Omega \left(G(\phi)\psi - \epsilon^2 \Delta \phi\right) d\mathbf{x} + \int_\Omega G(\phi)\psi\, d\mathbf{x} = 0$$

and

$$\frac{d\mathcal{E}_{IEQ}}{dt} = \int_\Omega \left(-\frac{\partial \phi}{\partial t} + \frac{1}{|\Omega|}\int_\Omega G(\phi)\psi \, d\mathbf{x} \right) \frac{\partial \phi}{\partial t} \, d\mathbf{x} = -\int_\Omega \left(\frac{\partial \phi}{\partial t} \right)^2 d\mathbf{x} \le 0.$$

Next, we utilize the SAV idea to obtain another EQ reformulation by introducing a scalar auxiliary variable $\psi(t) = \sqrt{\int_\Omega F(\phi)\, d\mathbf{x} + C}$, where C is a constant such that $\int_\Omega F(\phi)\, d\mathbf{x} + C > 0$. Then, one can redefine the energy $\mathcal{E}(\phi)$ as

$$\mathcal{E}_{SAV}(\phi, \psi) = \psi^2 + \int_\Omega \frac{\epsilon^2}{2} |\nabla \phi|^2 \, d\mathbf{x} - C \tag{5}$$

and reformulate Eq. (2) as

$$\frac{\partial \phi}{\partial t} = -\left(G(\phi)\psi - \epsilon^2 \Delta \phi \right) + \frac{1}{|\Omega|}\int_\Omega G(\phi)\psi \, d\mathbf{x}, \quad \frac{\partial \psi}{\partial t} = \frac{1}{2}\int_\Omega G(\phi)\frac{\partial \phi}{\partial t} \, d\mathbf{x}, \tag{6}$$

where $G(\phi) = \frac{f(\phi)}{\sqrt{\int_\Omega F(\phi)\, d\mathbf{x} + C}}$. The time derivatives of the mass and energy for the new system (6) can be computed in the same way as that for (4), which proves that the SAV scheme also satisfies the mass conservation and energy dissipation properties.

The auxiliary variable $\psi(\mathbf{x}, t)$ is a function of the space variable $\mathbf{x}$ and the time variable t in the IEQ reformulation, whereas the scalar auxiliary variable $\psi(t)$ only depends on the time variable t in the SAV reformulation. This slight difference leads to technical deviations in the mathematical proof and the numerical implementations; however, the two schemes share a principal similarity.

2.2. Energy quadratization Runge–Kutta scheme

Applying an s-stage RK method to the EQ reformulated system (4) or (6), we have the following EQ-RK scheme. For the RK coefficients $\mathbf{A} = (a_{ij}) \in \mathbb{R}^{s\times s}$ and $\mathbf{b} = (b_i), \mathbf{c} = (c_i = \sum_{j=1}^s a_{ij}) \in \mathbb{R}^s$,

$$\phi_i = \phi^n + \Delta t \sum_{j=1}^s a_{ij} p_j, \quad \psi_i = \psi^n + \Delta t \sum_{j=1}^s a_{ij} q_j, \tag{7}$$

where

$$\begin{aligned} p_i &= -\left(G(\phi_i)\psi_i - \epsilon^2 \Delta \phi_i \right) + \frac{1}{|\Omega|}\left(G(\phi_i), \psi_i \right), \; q_i = \frac{1}{2} G(\phi_i) p_i \qquad \text{for IEQ,} \\ p_i &= -\left(G(\phi_i)\psi_i - \epsilon^2 \Delta \phi_i \right) + \frac{1}{|\Omega|}\left(G(\phi_i), \psi_i \right), \; q_i = \frac{1}{2}\left(G(\phi_i), p_i \right) \quad \text{for SAV.} \end{aligned}$$

Here, $(\cdot, \cdot)$ denotes the L^2-inner product with respect to Ω. Then, ϕ^{n+1} and ψ^{n+1} are updated via

$$\phi^{n+1} = \phi^n + \Delta t \sum_{i=1}^s b_i p_i, \quad \psi^{n+1} = \psi^n + \Delta t \sum_{i=1}^s b_i q_i. \tag{8}$$

Definition 1 (*Stability Condition [18]*)**.** Define a symmetric matrix $\mathbf{M}$ given by

$$\mathbf{M} = \mathrm{diag}(\mathbf{b})\mathbf{A} + \mathbf{A}^T \mathrm{diag}(\mathbf{b}) - \mathbf{b}\mathbf{b}^T.$$

The stability condition is defined as

$$b_i \ge 0 \text{ for } i = 1, \ldots, s \text{ and } \mathbf{M} \text{ is positive semi-definite.} \tag{9}$$

The RK coefficients satisfying the stability condition (9) are listed in Table 1.

Table 1
Butcher tableaus of the diagonally implicit RK method [19,20].

first-order	second-order	third-order	fourth-order
$\begin{array}{c\|c} 1 & 1 \\ \hline & 1 \end{array}$	$\begin{array}{c\|cc} \frac{1}{2} & \frac{1}{2} \\ \hline & 1 \end{array}$	$\begin{array}{c\|cc} \sigma & \sigma & 0 \\ 1-\sigma & 1-2\sigma & \sigma \\ \hline & \frac{1}{2} & \frac{1}{2} \end{array}$	$\begin{array}{c\|ccc} \sigma & \sigma & 0 & 0 \\ \frac{1}{2} & \frac{1}{2}-\sigma & \sigma & 0 \\ 1-\sigma & 2\sigma & 1-4\sigma & \sigma \\ \hline & \mu & 1-2\mu & \mu \end{array}$
		$\sigma = \frac{3+\sqrt{3}}{6}$	$\sigma = \frac{\cos(\frac{\pi}{18})}{\sqrt{3}} + \frac{1}{2},\ \mu = \frac{1}{6(2\sigma-1)^2}$

Remark 2. Since the EQ-RK scheme is based on the RK method, we can achieve desired order of accuracy in time if we choose proper RK coefficients (such as given in Table 1). And, to make order of accuracy in space compatible with high-order in time, we employ the Fourier spectral method [21] for the numerical differentiation in (7)–(8).

Below, we show that the EQ-RK scheme with RK coefficients satisfying the stability condition is unconditionally energy stable.

Theorem 3. *The EQ-RK scheme (7)–(8) with RK coefficients satisfying the stability condition (9) is unconditionally stable with respect to the EQ reformulated energy $\mathcal{E}_{EQ}(\phi,\psi)$ in (3) or (5), meaning that for any time step $\Delta t > 0$,*

$$\mathcal{E}_{EQ}(\phi^{n+1},\psi^{n+1}) \le \mathcal{E}_{EQ}(\phi^n,\psi^n), \qquad \text{where EQ = IEQ or SAV.}$$

Proof. For IEQ, we have from Eqs. (7) and (8)

$$\begin{aligned} \|\psi^{n+1}\|^2 - \|\psi^n\|^2 &= 2\Delta t \sum_{i=1}^{s} b_i \left(q_i,\psi^n\right) + (\Delta t)^2 \sum_{i=1}^{s}\sum_{j=1}^{s} b_i b_j \left(q_i,q_j\right) \\ &= 2\Delta t \sum_{i=1}^{s} b_i \left(q_i,\psi_i\right) - (\Delta t)^2 \sum_{i=1}^{s}\sum_{j=1}^{s} m_{ij} \left(q_i,q_j\right). \end{aligned}$$

Because $\mathbf{M}$ is positive semi-definite,

$$\|\psi^{n+1}\|^2 - \|\psi^n\|^2 \le 2\Delta t \sum_{i=1}^{s} b_i \left(q_i,\psi_i\right) = \Delta t \sum_{i=1}^{s} b_i \left(G(\phi_i)\psi_i, p_i\right). \tag{10}$$

For SAV, because $\mathbf{M}$ is positive semi-definite and ψ_i only depends on t,

$$(\psi^{n+1})^2 - (\psi^n)^2 \le 2\Delta t \sum_{i=1}^{s} b_i q_i \psi_i = \Delta t \sum_{i=1}^{s} b_i \left(G(\phi_i)\psi_i, p_i\right). \tag{11}$$

And we obtain

$$\|\nabla\phi^{n+1}\|^2 - \|\nabla\phi^n\|^2 \le 2\Delta t \sum_{i=1}^{s} b_i \left(\nabla\phi_i, \nabla p_i\right) = -2\Delta t \sum_{i=1}^{s} b_i \left(\Delta\phi_i, p_i\right). \tag{12}$$

Adding (10) or (11) and (12) yields

$$\begin{aligned} \mathcal{E}_{EQ}(\phi^{n+1},\psi^{n+1}) - \mathcal{E}_{EQ}(\phi^n,\psi^n) &\le \Delta t \sum_{i=1}^{s} b_i \left(G(\phi_i)\psi_i - \epsilon^2\Delta\phi_i, p_i\right) \\ &= \Delta t \sum_{i=1}^{s} b_i \left(-p_i + \frac{1}{|\Omega|}\left(G(\phi_i),\psi_i\right), p_i\right) \\ &= -\Delta t \sum_{i=1}^{s} b_i \|p_i\|^2. \end{aligned}$$

Because $b_i \ge 0$ for $i = 1,\dots,s$, $\mathcal{E}_{EQ}(\phi^{n+1},\psi^{n+1}) - \mathcal{E}_{EQ}(\phi^n,\psi^n) \le 0$. This completes the proof. □

2.3. Numerical implementation

Using an s-stage diagonally implicit RK method for convenience of implementation, the EQ-RK scheme (7) can be rewritten as follows.

$$\phi_i - a_{ii}\Delta t\, p_i = S_i^1, \tag{13}$$
$$\psi_i - a_{ii}\Delta t\, q_i = S_i^2, \tag{14}$$

where $S_i^1 = \phi^n + \Delta t \sum_{j=1}^{i-1} a_{ij} p_j$ and $S_i^2 = \psi^n + \Delta t \sum_{j=1}^{i-1} a_{ij} q_j$. Eq. (14) can be simplified as follows.

$$\begin{aligned} -\frac{1}{2} G(\phi_i)\left(\phi_i - S_i^1\right) + \psi_i &= S_i^2 \quad \text{for IEQ,} \\ -\frac{1}{2}\left(G(\phi_i), \phi_i - S_i^1\right) + \psi_i &= S_i^2 \quad \text{for SAV.} \end{aligned} \tag{15}$$

To solve Eqs. (13) and (15), we develop a Newton-type fixed point iteration method for ϕ_i^{m+1}, ψ_i^{m+1} starting with $\phi_i^0 = \phi_{i-1}$, $\psi_i^0 = \psi_{i-1}$ as follows.

$$\begin{bmatrix} \mathcal{A}^m & \mathcal{B}^m \\ \mathcal{C}^m & \mathcal{I} \end{bmatrix} \begin{bmatrix} \phi_i^{m+1} - \phi_i^m \\ \psi_i^{m+1} - \psi_i^m \end{bmatrix} = \begin{bmatrix} S_i^1 - \mathcal{N}^1(\phi_i^m, \psi_i^m) \\ S_i^2 - \mathcal{N}^2(\phi_i^m, \psi_i^m) \end{bmatrix}, \tag{16}$$

where

$$\begin{aligned} &\mathcal{A}^m = \mathcal{I} + a_{ii}\Delta t \left(G'(\phi_i^m)\psi_i^m - \epsilon^2 \Delta - \frac{1}{|\Omega|}\left(G'(\phi_i^m)\psi_i^m, \cdot\right)\right), \\ &\mathcal{B}^m = a_{ii}\Delta t \left(G(\phi_i^m) - \frac{1}{|\Omega|}\left(G(\phi_i^m), \cdot\right)\right), \\ &\left(G'(\phi_i^m)\psi_i^m, \cdot\right)\phi := \left(G'(\phi_i^m)\psi_i^m, \phi\right), \quad \left(G(\phi_i^m), \cdot\right)\psi := \left(G(\phi_i^m), \psi\right), \\ &\mathcal{N}^1(\phi, \psi) = \phi + a_{ii}\Delta t \left(G(\phi)\psi - \epsilon^2 \Delta\phi - \frac{1}{|\Omega|}\left(G(\phi), \psi\right)\right), \end{aligned}$$

and

$$\begin{aligned} &\mathcal{C}^m = -\frac{1}{2}\left(G(\phi_i^m) + G'(\phi_i^m)\left(\phi_i^m - S_i^1\right)\right), \quad \mathcal{N}^2(\phi, \psi) = -\frac{1}{2} G(\phi)\left(\phi - S_i^1\right) + \psi, \\ &G'(\phi) = \frac{2f'(\phi)(F(\phi) + C) - (f(\phi))^2}{2(F(\phi) + C)^{\frac{3}{2}}} \qquad \text{for IEQ,} \\ &\mathcal{C}^m = -\frac{1}{2}\left(G(\phi_i^m) + G'(\phi_i^m)\left(\phi_i^m - S_i^1\right), \cdot\right), \quad \mathcal{N}^2(\phi, \psi) = -\frac{1}{2}\left(G(\phi), \phi - S_i^1\right) + \psi, \\ &G'(\phi) = \frac{2f'(\phi)((F(\phi), \mathbf{1}) + C) - f(\phi)(f(\phi), \mathbf{1})}{2((F(\phi), \mathbf{1}) + C)^{\frac{3}{2}}} \quad \text{for SAV.} \end{aligned}$$

The system (16) can be further simplified as follows.

$$\left(\mathcal{A}^m - \mathcal{B}^m\mathcal{C}^m\right)\left(\phi_i^{m+1} - \phi_i^m\right) = S_i^1 - \mathcal{N}^1(\phi_i^m, \psi_i^m) - \mathcal{B}^m(S_i^2 - \mathcal{N}^2(\phi_i^m, \psi_i^m)), \tag{17}$$
$$\psi_i^{m+1} = \psi_i^m + S_i^2 - \mathcal{N}^2(\phi_i^m, \psi_i^m) - \mathcal{C}^m(\phi_i^{m+1} - \phi_i^m). \tag{18}$$

We solve ϕ_i^{m+1} using Eq. (17) and then update ψ_i^{m+1} by Eq. (18), and set

$$\phi_i = \phi_i^{m+1} \quad \text{and} \quad \psi_i = \psi_i^{m+1}$$

if a relative l_2-norm of the consecutive error $\frac{\|\phi_i^{m+1} - \phi_i^m\|}{\|\phi_i^m\|}$ is less than a tolerance tol_{n}. In this study, the biconjugate gradient (BICG) method is used to solve Eq. (17), and we use the following preconditioner $\mathcal{P}$ to accelerate the convergence speed of the BICG algorithm: $\mathcal{P} = \mathcal{I} + a_{ii}\Delta t\left(-\epsilon^2\Delta\right)$. The stopping criterion for the BICG iteration is that the relative residual norm is less than tol_{bicg}.

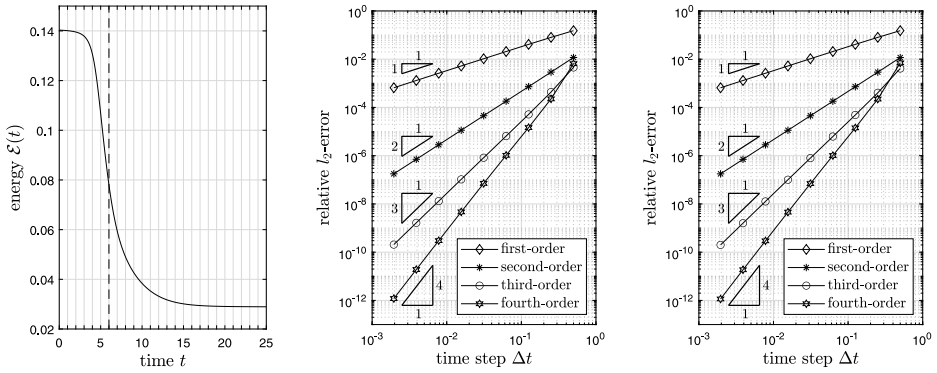

(a) Reference Solution (b) **IEQ** Convergence (c) **SAV** Convergence

Fig. 1. (a) Evolution of $\mathcal{E}(t)$ for the reference solution with $\epsilon = 0.01$ and $h = \frac{1}{128}$. (b)–(c) Convergence of $\phi(x, y, t = 6)$ by the EQ-RK schemes.

3. Numerical experiments

Unless otherwise stated, we set $\epsilon = 0.01$, $C = 1$, $h = \frac{1}{128}$, $tol_{\mathrm{n}} = 10^{-6}\Delta t$, and $tol_{\mathrm{bicg}} = 10^{-8}\Delta t$ for the simulations in this section.

3.1. Numerical convergence with a smooth test function in 2D

We demonstrate the convergence of proposed scheme with an initial condition

$$\phi(x, y, 0) = 0.02\cos(4\pi x)\cos(3\pi y) + 0.1\cos(3\pi x)\cos(2\pi y) - 0.5$$

on $\Omega = [0, 1] \times [0, 1]$. To estimate the convergence rate with respect to Δt, simulations are performed by varying $\Delta t = 2^{-9}, 2^{-8}, \ldots, 2^{-1}$. We take the quadruply over-resolved numerical solution using the fourth-order scheme as the reference solution. Fig. 1(a) shows the evolution of $\mathcal{E}(t)$ for the reference solution. For IEQ and SAV, the relative l_2-errors of $\phi(x, y, 6)$ for various time steps are shown in Figs. 1(b) and (c), respectively. Here, the errors are computed by comparison with the reference solution. We note that the proposed scheme provides the desired order of accuracy in time.

For IEQ, to demonstrate the robustness of the nonlinear solver, we count the number of nonlinear and BICG iterations (see Fig. 2). Here, we regard the number of BICG iterations at each time level as the average number of BICG iterations for the nonlinear iterations at each time level. For the first- and second-order schemes, 2–3 nonlinear iterations were involved in proceeding to the next time level, and we believe that such a fast iterative convergence can be achieved since the successive iteration (17) is a Newton-type fixed point iteration method. Additionally, the numbers of nonlinear iterations of the (two-stage) third- and (three-stage) fourth-order schemes are approximately two and three times more than that of the (one-stage) first-order scheme, respectively. These results indicate that the number of nonlinear iterations is almost linear with respect to the number of stages. Furthermore, the BICG algorithm converges in a small number of iterations by using the preconditioner. We have not included figures for SAV but obtained results similar to those in Fig. 2.

3.2. Energy stability with a nonsmooth test function in 2D

To investigate the energy stability of proposed scheme, we take an initial condition as

$$\phi(x, y, 0) = -0.5 + \mathrm{rand}(x, y)$$

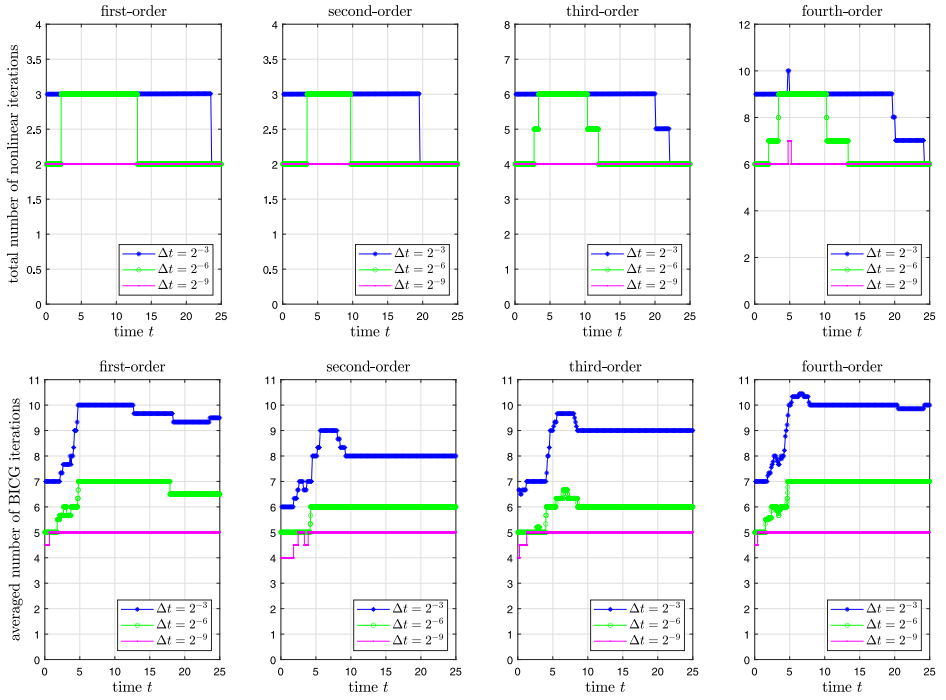

Fig. 2. Number of nonlinear and BICG iterations for the first-, second-, third-, and fourth-order **IEQ** schemes with different time steps.

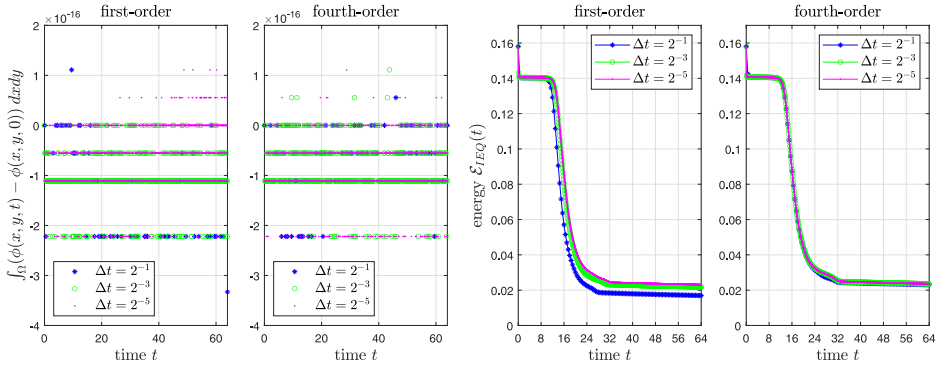

Fig. 3. Evolution of $\int_\Omega(\phi(x,y,t)-\phi(x,y,0))\,dxdy$ and $\mathcal{E}_{IEQ}(t)$ using the first- and fourth-order **IEQ** schemes with different time steps.

on $\Omega = [0,1]\times[0,1]$, where rand$(x,y)$ is a random number between -0.1 and 0.1 at the grid points. For IEQ, Fig. 3 shows the evolution of $\int_\Omega(\phi(x,y,t)-\phi(x,y,0))\,dxdy$ and $\mathcal{E}_{IEQ}(t)$ using the first- and fourth-order schemes with different time steps. Here, $\int_\Omega(\phi(x,y,t)-\phi(x,y,0))\,dxdy$ is approximated by $\sum\sum(\phi^n-\phi^0)\,\Delta x\Delta y$. We note that the mass fluctuation is roughly equal to the machine precision, which is considerably smaller than the numerical solution accuracy, and all the energy curves are nonincreasing over time (again in machine precision) owing to the mass conservation. For second-, third-order IEQ and SAV, we obtain results similar to those in Fig. 3.

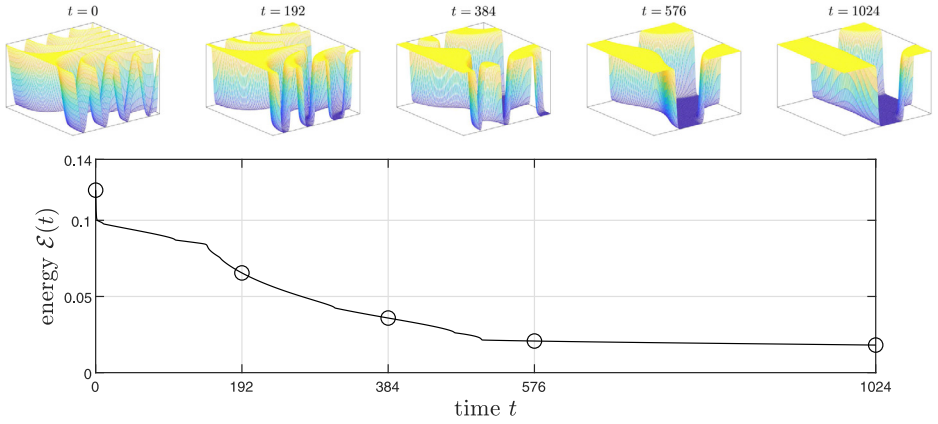

Fig. 4. Evolution of the reference solution $\phi(x, y, t)$ by the **SAV** scheme with $\epsilon = 0.01$ and $h = \frac{1}{128}$ and its original energy $\mathcal{E}(t)$.

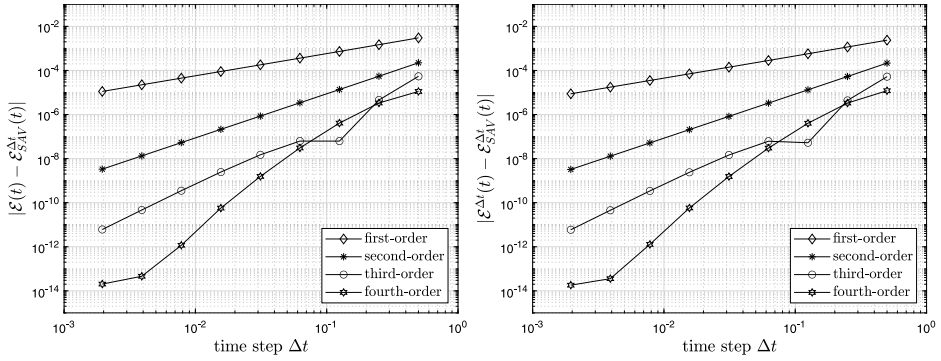

Fig. 5. Convergence of $\mathcal{E}_{SAV}^{\Delta t}(t)$ and differences between the original $\mathcal{E}^{\Delta t}(t)$ and the discrete $\mathcal{E}_{SAV}^{\Delta t}(t)$ energies by the **SAV** scheme at $t = 192$ for $\Delta t = 2^{-9}, 2^{-8}, \ldots, 2^{-1}$.

3.3. Energy convergence with a smooth test function in 2D

The original energy $\mathcal{E}(t)$ in (1) and the EQ reformulated energy $\mathcal{E}_{EQ}(t)$ in (3) or (5) are equivalent in the continuous-time case but not in the discrete-time case. To numerically quantify the difference between the discrete energies, we take an initial condition as

$$\phi(x, y, 0) = \cos\left(8\pi \min\left\{\sqrt[4]{(x-1)^4 + (|2y-1|-1)^4}, 1\right\}\right)$$

on $\Omega = [0, 1] \times [0, 1]$. The evolution of the reference solution $\phi(x, y, t)$ using the fourth-order SAV scheme with $\Delta t = 2^{-11}$ and its original energy $\mathcal{E}(t)$ using the reference solution is shown in Fig. 4. The coarsening dynamics and energy dissipation may be observed.

To clarify the difference between the continuous energy $\mathcal{E}(t)$ and EQ reformulated energy $\mathcal{E}_{EQ}(t)$, we define the continuous energy $\mathcal{E}(t) := \mathcal{E}(\phi(t))$ using the reference solution, the numerically computed original energy $\mathcal{E}^{\Delta t}(t^n) := \mathcal{E}(\phi(t^n))$, and the SAV reformulated energy $\mathcal{E}_{SAV}^{\Delta t}(t^n) := \mathcal{E}_{SAV}(\phi(t^n), \psi(t^n))$ with a time step Δt. In Fig. 5(a), $|\mathcal{E}(t) - \mathcal{E}_{SAV}^{\Delta t}(t)|$ clearly shows that the numerically computed SAV energy converges to the original energy in the desired order of accuracy, as expected. More interesting is the difference $|\mathcal{E}^{\Delta t}(t) - \mathcal{E}_{SAV}^{\Delta t}(t)|$ between the original and SAV energies using the computed solution at $t = 192$. Here, we note that the SAV energy differs from the original energy but is consistent with the order of numerical scheme accuracy. For IEQ, we obtain results similar to those in Figs. 4 and 5.

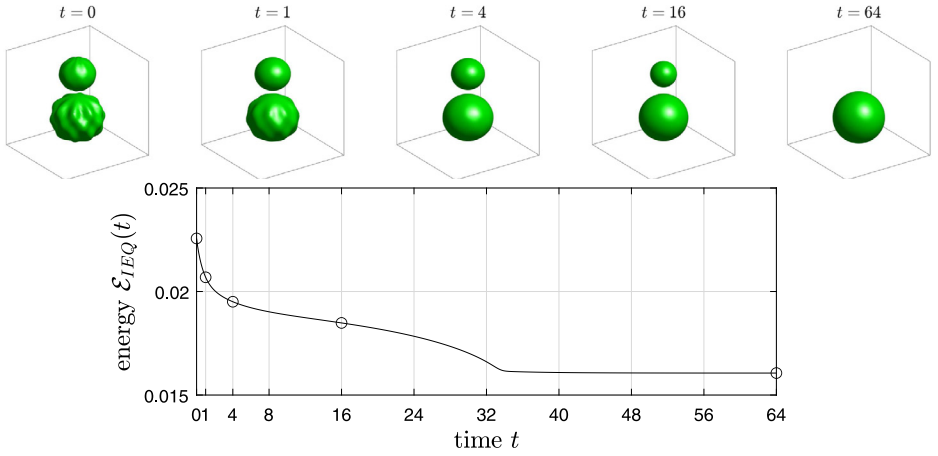

Fig. 6. Evolution of $\phi(x, y, z, t)$ and $\mathcal{E}_{IEQ}(t)$ using the fourth-order **IEQ** scheme with $\epsilon = 0.02$ and $h = \frac{1}{64}$.

3.4. Evolution of spheres perturbed by spherical harmonics in 3D

We perform the evolution of spheres perturbed by spherical harmonics on $\Omega = [0, 1] \times [0, 1] \times [0, 1]$ with $\epsilon = 0.02$, $h = \frac{1}{64}$ and $\Delta t = \frac{1}{8}$. An initial condition is as follows.

$$\phi(x, y, z, 0) = 1 + \sum_{i=1}^{2} \tanh\left(\frac{0.25 + s_i Y_{10}^8(\theta, \varphi) - r_i}{2\epsilon}\right),$$

where $(s_1, s_2) = (0.05, 0.01)$, $Y_{10}^8(\theta, \varphi)$ is a spherical harmonic with the polar θ and azimuthal φ angles, and $r_i = \sqrt{(x - 0.5)^2/a_i + (y - 0.5)^2/b_i + (z - z_i)^2/c_i}$ is the scaled radius with $(a_1, b_1, c_1, z_1) = (1, 1, 0.8, 0.35)$ and $(a_2, b_2, c_2, z_2) = (0.5, 0.5, 0.4, 0.8)$. For IEQ, Fig. 6 shows the evolution of $\phi(x, y, z, t)$ and $\mathcal{E}(t)$. As the energy is dissipated in time, each perturbed sphere evolves to a sphere in moving convex and concave parts inward and outward, respectively, and then two spheres merge into one. For SAV, we obtain results similar to those in Fig. 6.

4. Conclusions

We developed a high-order (up to fourth-order) energy stable EQ-RK scheme for the CAC equation with a nonlocal Lagrange multiplier. Additionally, we implemented the EQ-RK scheme by using the Newton-type fixed point iteration method. Under the stability condition for the RK coefficients, unconditional energy stability of the EQ-RK scheme was proven theoretically. We numerically confirmed that the EQ-RK scheme yields the desired order of accuracy in time and is unconditionally stable with respect to the EQ reformulated energy, and that the discrete version of the EQ reformulated energy is a high-order approximation of the original energy.

Acknowledgment

This research was supported by the National Research Foundation of Korea (NRF) grant funded by the Ministry of Science and ICT of Korea (MSIT) (No. 2019R1A6A1A11051177, 2019R1C1C1011112, 2020R1C1C1A01013468).

References

[1] L.-Q. Chen, Phase-field models for microstructure evolution, Annu. Rev. Mater. Res. 32 (2002) 113–140.
[2] J.W. Cahn, J.E. Hilliard, Free energy of a nonuniform system. I. Interfacial free energy, J. Chem. Phys. 28 (1958) 258–267.
[3] S.M. Allen, J.W. Cahn, A microscopic theory for antiphase boundary motion and its application to antiphase domain coarsening, Acta Metall. 27 (1979) 1085–1095.
[4] J. Rubinstein, P. Sternberg, Nonlocal reaction–diffusion equations and nucleation, IMA J. Appl. Math. 48 (1992) 249–264.
[5] M. Brassel, E. Bretin, A modified phase field approximation for mean curvature flow with conservation of the volume, Math. Methods Appl. Sci. 34 (2011) 1157–1180.
[6] J. Kim, S. Lee, Y. Choi, A conservative Allen–Cahn equation with a space–time dependent Lagrange multiplier, Int. J. Eng. Sci. 84 (2014) 11–17.
[7] S. Kwak, J. Yang, J. Kim, A conservative Allen–Cahn equation with a curvature-dependent Lagrange multiplier, Appl. Math. Lett. 126 (2022) 107838.
[8] J. Shen, X. Yang, An efficient moving mesh spectral method for the phase-field model of two-phase flows, J. Comput. Phys. 228 (2009) 2978–2992.
[9] J. Shen, X. Yang, A phase-field model and its numerical approximation for two-phase incompressible flows with different densities and viscosities, SIAM J. Sci. Comput. 32 (2010) 1159–1179.
[10] M. Beneš, S. Yazaki, M. Kimura, Computational studies of non-local anisotropic Allen–Cahn equation, Math. Bohem. 136 (2011) 429–437.
[11] M. Okumura, A stable and structure-preserving scheme for a non-local Allen–Cahn equation, Japan J. Indust. Appl. Math. 35 (2018) 1245–1281.
[12] J. Shen, X. Yang, A novel fully decoupled scheme with second-order time accuracy and unconditional energy stability for the Navier–Stokes equations coupled with mass-conserved Allen–Cahn phase-field model of two-phase incompressible flow, Internat. J. Numer. Methods Engrg. (2020) 1–24.
[13] X. Yang, Linear, first, second order, Unconditionally energy stable numerical schemes for the phase field model of homopolymer blends, J. Comput. Phys. 327 (2016) 294–316.
[14] J. Shen, J. Xu, J. Yang, The scalar auxiliary variable (SAV) approach for gradient flows, J. Comput. Phys. 353 (2018) 407–416.
[15] C. Yao, H. Fan, Y. Zhao, Y. Shi, F. Wang, Fast algorithm for nonlocal Allen–Cahn equation with scalar auxiliary variable approach, Appl. Math. Lett. 126 (2022) 107805.
[16] N. Zheng, X. Li, New efficient and unconditionally energy stable schemes for the Cahn–Hilliard–Brinkman system, Appl. Math. Lett. 128 (2022) 107918.
[17] Y. Gong, J. Zhao, Energy-stable Runge–Kutta schemes for gradient flow models using the energy quadratization approach, Appl. Math. Lett. 94 (2019) 224–231.
[18] J.C. Butcher, Numerical Methods for Ordinary Differential Equations, John Wiley & Sons, 2016.
[19] E. Hairer, S.P. Norsett, G. Wanner, Solving Ordinary Differential Equations I: Nonstiff Problems, Springer, 1993.
[20] E. Hairer, G. Wanner, Solving Ordinary Differential Equations II: Stiff and Differential-Algebraic Problems, Springer, 1996.
[21] J. Shin, H.G. Lee, J.-Y. Lee, Long-time simulation of the phase-field crystal equation using high-order energy-stable CSRK methods, Comput. Methods Appl. Mech. Engrg. 364 (2020) 112981.